DR. WOLFGANG GÄRTNER (Orcid ID : 0000-0002-6898-7011)

DR. VIRGINIA ALBARRACIN (Orcid ID : 0000-0002-4316-0720)

Article type : Special Issue Research Article

Photolyases and Cryptochromes in UV-resistant Bacteria from High-altitude Andean Lakes†

Luciano Raúl Portero[1,2]; Daniel Alonso[1,2]; Federico Zannier[1,2]; Martín P. Vazquez[3], María Eugenia Farías[1], Wolfgang Gärtner[5]and Virginia Helena Albarracín[1,2,4]*

[1]Laboratorio de Investigaciones Microbiológicas de Lagunas Andinas (LIMLA), Planta Piloto de Procesos Industriales y Microbiológicos (PROIMI), CCT, CONICET, Tucumán, Argentina.
[2]Centro Integral de Microscopía Electrónica (CIME, CONICET, UNT) CCT, CONICET, Tucumán, Argentina.
[3]Instituto de Agrobiotecnología de Rosario (INDEAR), Predio CCT Rosario, Santa Fe, Argentina
[4]Facultad de Ciencias Naturales e Instituto Miguel Lillo, Universidad Nacional de Tucumán, Tucumán, Argentina.
[5]Institute for Analytical Chemistry, University of Leipzig, Germany

†This article is part of a Special Issue celebrating Photochemistry and Photobiology's 55th Anniversary.

Running headline: PHOTORECEPTORS IN UV-RESISTANT BACTERIA.

Keywords: photoreceptors, photolyases, cryptochromes, extremophiles, *Exiguobacterium*, *Acinetobacter*, *Nesterenkonia*

This article has been accepted for publication and undergone full peer review but has not been through the copyediting, typesetting, pagination and proofreading process, which may lead to differences between this version and the Version of Record. Please cite this article as doi: 10.1111/php.13061

*Corresponding author's email: viralbarracin@gmail.com (Virginia Helena Albarracín)

ABSTRACT

"High-Altitude Andean Lakes" (HAAL) are pristine environments harboring poly-extremophilic microbes that show combined adaptations to physical and chemical stress such as large daily ambient thermal amplitude, extreme solar radiation levels, intense dryness, alkalinity, high concentrations of arsenic (up to 200 ppm) and dissolved salts. In this work, we compared the UV resistance profiles, pigment content and photoreactivation abilities of three UV-resistant bacteria isolated from distinct niches from HAAL´s: i.e. *Acinetobacter* sp. Ver3 (water, Lake Verde; 4.400 m), *Exiguobacterium* sp. S17 (stromatolite, Lake Socompa, 3,570 m) and *Nesterenkonia* sp. Act20 (soil, Lake Socompa, 3,570 m).

UV resistance ability of HAAL´s strains indicate a clear adaptation to high radiation exposure encountered in their original habitat, which can be explained by genetic and physiological mechanisms named as the UV-resistome. Thus, the UV-resistome depends on the expression of a diverse set of genes devoted to evading or repairing the damage it provoked direct or indirectly. As pigment extraction and photoreactive assays indicate the presence of photoactive molecules, we characterized more in detail proteins with homology to photolyases/cryptochromes members (CPF). Phylogenetic analyses, sequence comparison and 3D modelling with bonafide CPFs members was used to proof the presence of functional domains and key residues in the novel proteins.

INTRODUCTION

The Central Andes region displays unexplored ecosystems of shallow lakes and salt flats at altitudes between 3,000 and 6,000 m called as "High-Altitude Andean Lakes" (HAAL). These pristine environments are a rich source of poly-extremophilic microbes that shows combined adaptations to physical and chemical stress: i.e. large daily ambient thermal amplitude, extreme solar radiation levels, intense dryness, alkalinity, high concentrations of arsenic (up to 200 ppm) and dissolved salts (1,2). Of particular importance is the high solar irradiance in the HAAL (1,2) with values of UV-B flux at mid-day up to 10 W m^{-2} and a monthly average of daily insolation of 6.6 $kWhm^{-2}$ d^{-1}; these parameters are among the highest in the world (3) (NASAOMI/Aura Online serverhttp://gdata1.sci.gsfc.nasa.gov). The radiation values on HAALs are 165% higher than the reported values for lakes at sea level (1,2,4–9), and the erythemal index[1] extends above to 15, which is equivalent to 5.57 MED[2] h^{-1} and to ca. 1200 J m^{-2} h^{-1}. The low latitude and high altitude at HAAL is responsible for a thin ozone layer and a clear sky that favor intense UV radiation, a pattern which is clearly observed in lakes such as the one on the summit of the Licancabur volcano (5,917 m) and Laguna Blanca (4,340 m) (Bolivia) (8,9).

According to the Comité Internationale de l'Eclairage (CIE), the ultraviolet part of the electromagnetic spectrum is subdivided into ultraviolet A (UV-A) (315–400 nm), UV-B (280–315 nm) and UV-C (<280 nm) (CIE, 2011). As solar UV-C spectrum is filtered by the atmospheric gases O_2, H_2O, CO_2 and mainly O_3, UV range affecting life on Earth falls only

[1] The World Meteorological Organization has established one UV Index Unit at 25 mW m^{-2} or 90 J m^{-2} h^{-1}.

[2] The erythematic dose Minim (MED) is defined as the unit of weighted UV-B radiant energy that produces a barely perceptible erythema on the skin (clear skin) and is equivalent to 210 J m^{-2}. 1 MED / hour is defined as the ratio (irradiance itself) with which UV-B radiation affects some surface.

between 280 to 400 nm. The UV-A spectrum constitutes 95% of UV-spectrum that reaches the earth causing cell damage indirectly by causing photooxidation of compounds and generating reactive oxygen species (10,11). In turn, UV-B represent less than 5% of incident solar radiation; besides triggering oxidative damage UV-B also is able to excite and ionize biologically relevant molecules, such as lipids, proteins and DNA, causing the formation of different types of photoproducts (Pho) (12). DNA damage produced by UV-B irradiation reproduced by dimerization or adduct formation between adjacent pyrimidines bases (Thymine or Cytosine) on one DNA strand. The dimerization products called as cyclobutane pyrimidine dimers (CPDs) constitute 70-80% of total photoproducts while the adducts accounted for the rest and are termed 6–4[pyrimidine-2′-one] pyrimidines or (6-4)photoproducts ((6–4)PPs) (12,13). Photoproducts (6-4) can be transformed to "Dewar photoisomers" through UV-A, UV-B and UV-C radiation. The biological effects are very variable depending on the type and extent of mutation produced.

Indigenous microorganisms originally isolated from irradiated environment are in general well adapted to high UV exposure (14–20). This is also the case for HAAL's strains that display intrinsically high UV resistance and are now considered novel models for studying adaptive responses and mechanisms of light sensing and UV–triggered mechanisms (1,2,21). Genes encoding photoreceptors were identified in these strains, and a CPD class I photolyase from *Acinetobacter* sp. Ver3 was functionally characterized (22). These results call for a deeper screening in strains from HAAL and request a more detailed characterization of HAAL's novel bacterial photoreceptors that already were coined extremo-enzymes.

Among many mechanisms that bacteria have developed to counteract high UV-radiation, DNA repair systems are essential as they enable cells to cope with fatal DNA damage. These mechanisms are usually classified in dark repair (DR) and photo repair (PR) (23,24). This last mechanism -also called photoreactivation- allows cells to repair UV-

induced damage in their DNA upon adequate light irradiation for a certain time by using an enzyme called photolyase activated by light in the UV-A and blue-light range (25).

Photolyases (Phr) together with the structurally closely related cryptochromes (Cry) form a divergent family of photoactive proteins present in all three biological domains of life, called as cryptochrome/photolyase family (CPF). This includes monomeric flavoproteins of 53-66 kDa, containing between 450 and 620 amino acids, and a non-covalently bound flavin adenine dinucleotide (FAD) as cofactor in a 1:1 ratio. Some members of this protein family also carry an antenna pigment, such as deazaflavin, lumazin, or methenyltetrahydrofolate derivatives (26–28). Cry and Phr proteins share a large percentage of sequence identity, and their 3D-structures are very similar, probably due to their origin from a common ancestor (29).

Photolyases are classified according to the type of repaired photoproduct i.e. cyclobutane pyrimidine dimer (CPD-Phr) photolyases, or (6–4) pyrimidine-pyrimidone photolyases (6-4-Phr). Cryptochromes (Cry) have no photolyase activity and function as signaling molecules regulating diverse biological responses such as entrainment of circadian rhythms in plants and animals (30,31). According to Oberpichler 2011 (32), seven groups can be distinguished within the CPF: CPD class I; CPD class II; CPD class III; (6-4) photolyase and animal Cry; plant Cry; Cry-DASH; FeS-BCP (including the minor clusterCry-Pro). The (6-4) photolyases are very similar to animal Cry; the Plant Cry is the sister group of CPD class III, which is more often found in bacteria. Recently, CryDASHwas described to be able to bind flavin adenine dinucleotide that can be photoreduced by blue light; also, CryDASH has been reported to binds single-stranded DNA with very high affinity (*K*d ~10^{-8} M), and double-stranded DNA and single-stranded RNA with far lower affinity (*K*d ~10^{-6} M). Cry-DASH was found to repair CPDs specifically in single-stranded DNA (ssDNA) (33,34), so these proteins should be coined photolyases. Other studies showed that the CPF must be

expanded by an additional class called as Fe-S bacterial cryptochromes and photolyases (FeS-BCPs), in which members carry a 4Fe4S cluster (32).

In this work, we compare the UV resistance profiles, photoreactivation abilities and pigment content of three UV-resistant bacteria originally isolated from distinct niches from HAALs: i.e. *Acinetobacter* sp. Ver3 (22,38) (water, Lake Verde; 4,400 m), *Exiguobacterium* sp. S17 (stromatolite, Lake Socompa, 3,570 m) (37) and *Nesterenkonia* sp. Act20 (21) (soil, Lake Socompa, 3,570 m) for which genomes sequences are available (35–37). Considering the high UV-resistance phenotype of HAAL's strains, these genomes were screened for the presence and diversity of sequences with homology to CPFs members. In addition, 3D modeling and a phylogenetic comparison with other known bacterial CPF sequences were performed.

MATERIALS AND METHODS

Strains and culture conditions. UV-resistant strains used in this study were previously isolated from different HAALs at the Andean Puna in Argentina (1,2), belonging to the LIMLA-PROIMI Extremophilic Strain Collection.

Acinetobacter sp. Ver3 was isolated from the Andean Lake Verde (4,400 m); *Exiguobacterium* sp. S17 was isolated from a Lake Socompa stromatolite (3,570 m) (17,35,38), and *Nesterenkonia* sp. Act20 was isolated from soil around Lake Socompa (3,570 m) (21). Bacterial strains from DSMZ Bacterial Culture Collection were used as UV sensitive controls as was previously reported (19,21,39) (**Fig. 1**), they were: *Acinetobacter johnsonii* DSM 6963, *Acinetobacter baumannii* DSM 30007, *Acinetobacter lwoffi* DSM 2463, *Exiguobacterium aurantiacum* DSM 6208, and *Nesterenkonia halotolerans* DSM 15474.

Acinetobacter spp. and *Exiguobacterium* spp. were grown in Luria–Bertani (LB) broth, supplemented with 2% agar for solid medium when applicable. *Nesterenkonia* strains were grown in "H" medium (a medium modified for halophiles, containing NaCl 15g/L, KCl 3g/L, $MgSO_4$ 5g/L, sodium citrate 3 g/L) added with 2% agar for solid medium when applicable.

For electron microscopy, aliquots of a stationary state-culture of each strain were fixed overnight at 4 °C in Karnovsky's fixative, comprising formaldehyde (8 % v/v), glutaraldehyde (16 % v/v), and phosphate-buffered saline (PBS; 0.2 M, pH 7.4). The fixed samples were washed three times with phosphate buffer for 10 min. Later, they were fixed with 2 % v/v osmium tetroxide overnight. The samples were dehydrated successively with increasing alcohol concentrations (30%, 50%, 70%, 90%, 100%) for 10 min each and finally maintained in acetone for 24 h. The final dehydration was carried out with the critical point technique. Samples were mounted on scanning electron microscopy sample stubs and gold coated. Specimens were observed under vacuum using a Zeiss Supra 55VP (CarlZeissNTS GmbH, Germany) scanning electron microscope.

UV-B resistance assays. For a quick and qualitative determination of level of resistance to different UV-B irradiation doses the assays were performed on agar media. Briefly, cultures were collected at OD_{600nm} of 0.6 and subjected to serial dilutions. Aliquots of 5 µL were then loaded onto medium agar plates, (the petri plates were covered with acetate film to block out UV-C), and, once inoculated, were immediately exposed to UV-B lamps (Vilbert Lourmat VL-4, maximum intensity at 312 nm) as light source (see lamp spectra, Supporting Information, Supplementary File S1) covered by acetate sheet (see spectra, Supporting Information, Supplementary File S2). As Gram-negative strains are much more UV-sensitive than Gram-positive strains (18,19,39), different duration and irradiation doses were applied

depending on the strain. *Acinetobacter* strains were exposed to 15, 30, 60, 120, 180, and 240 minutes of UV-B irradiation at 2.98 W/m^2, while *Exiguobacterium* and *Nesterenkonia* strains were exposed to 5.4 W/m^2 during different times (0, 60, 90, and 120 minutes). Then, the strains were incubated in the dark to prevent photoreactivation, for 24, 48 and 72 h at 30 ºC. Microbial growth was recorded with three positive signs (+++) when it was similar to the growth in the control, with two positive signs (++) when it was slightly different from the growth in the control, with one positive sign (+) when the growth was too low to allow colony counting, with a negative sign (-) when no growth at all was observed. For plotting the data in a graphic, three, two or one sign was taken as 3, 2 or 1 unit of growth for each dilution and then summed up together to reach a unique value. Negative signs were counted as null unit of growth.

Photoreactivation assays. To evaluate the UV-B photo repair ability, selected strains were grown in LB medium at 30 °C with shaking (2.3 g). Cells were harvested in the mid-exponential phase by centrifugation at 10,700g for 20 min at 4 °C. The cell pellets were washed twice in 0.9 % NaCl and were kept under starvation conditions in the same solution for 12 h at 4 °C. A 20 mL portion of each cell suspension (at OD_{600} 0.6) was transferred to 45-ml sterile quartz tubes, these were covered with acetate film to block out UV-C and then exposed to UV-B radiation at an irradiance of 5.4 W m^{-2}, until microbial growth decreased to ca. 50% (CFUs) of the strain under study with shaking (50 rpm) at 15 °C. Controls were incubated under the same conditions, but in the dark. After UV-B exposure, 100 µL of the cell culture were removed from the tubes and microbial growth was assessed upon growth in solid medium (CFUs) after 48 h of incubation at 30 °C in the dark to prevent photoreactivation. Aliquots from UV-B exposed cell suspensions were subjected to photo repair (PR) or dark repair (DR) conditions. Photo repair was allowed by incubating the suspensions under photosynthetically active radiation (PAR) during 120 min (18 Wm^{-2}),

using OSRAM L18 W/77 lamps with continuous shaking (0.13 g) at 15 °C, while dark repair was evaluated under the same experimental conditions but without PAR illumination. After each treatment, 100 µL cells were removed from the tubes and the number of CFUs was determined after 48 h of incubation at 30 °C under dark conditions to prevent photoreactivation. Incubation in the dark was accomplished by covering the quartz tubes or agar plates with aluminum foil.

Statistical analysis. Each experiment consisted of three biological replicas, error bars are the standard deviation (Ơ 2). The means and the standards error of both, UV resistance profiles and photorepair ability assays, were assessed through Microsoft Excel statistical functions of three biological repetitions of each experiment.

Pigments extraction. Pellets of 150 mL of Act20, S17, and Ver3 cultures grown for 3 days were harvested through centrifugation at 10,700g for 10 min, washed twice with physiological solution (PS), and centrifuged again. Pigments from the pellets were first extracted with aliquots of a mix of 2 ml methanol and 1 ml acetone (2:1), mixed with a vortex, and left at rest for 2 min. Pellets were centrifuged at 10,700 g pm, the supernatant was collected with a Pasteur pipette, filtered, and transferred to a clean tube. The procedure was repeated twice. For the complete extraction of the pigments, the procedure was repeated with 2 ml acetone, 2 ml methanol, and 2 ml hexane, one solvent at a time. The mixed solution was concentrated with nitrogen at low pressure and room temperature. Then, the sample was washed with 3 ml of PS and 3 ml of diethylether (DEE). The diethylether phase was collected and, in order to release carotenoids from conjugated groups (i.e glycosides), a step of saponification was performed by adding 1:1 10% methanolic sodium hydroxide and incubation for 6 hours protected from the light. The solution was dried with nitrogen as

above, washed with PS and pigments re-extracted with DEE. The pigments absorption spectra were recorded with Elisa Reader spectrophotometer (Multiskan Go, Thermoscientific) from 200 to 700 nm using DEE as blank all-trans-Astaxanthin, Canthaxanthin and β-Carotene (all of them from SIGMA)

Sequence comparison and phylogenetic analyses. Genomes of *Acinetobacter* sp. Ver3 and *Exiguobacterium* sp. S17 are available at the NCBI database under accession numbers GCA_000632455.1 and GCA_000411915.1 respectively (40,41). Using the BLAST tool and sequences of CPF family described in previous works, we found putative candidates encoding photoreceptors in the HAAL isolates (Ver3; Act20; S17). The sequences of the two photoreceptors found in Act20 genome (unpublished) were individually uploaded in Genbank (42), with accession numbers MG800787 and MG800788. RAST annotated genomes for all three strains were inspected searching for genes related with the UV-Resistome (see Supporting Information, Supplementary File S2).

Phylogenetic tree was constructed using 45 bacterial sequences of the CPF family retrieved from the NCBI and Uniprot-KB databases in which experimental work proved their function as photolyase or cryptochrome (Table S1). A larger phylogenetic tree was constructed using186 CPF homologues bacterial sequences, including the small dataset of know function of the first tree together with sequences with high identity retrieved from the NCBI and Uniprot-KB databases (Table S2). Multiple alignment was performed with ClustalX, main tree was generated with Neighbor-joining (NJ) method using MEGA7 program (35) and the larger phylogenetic tree using FastME 2.0 (43), with 1000 bootstrap replicates. Subsequent processing and visualization was performed using iTOL (http://itol.embl.de/). Eight sequences were selected from the main set in order to trace the evolution of the family using Maximum Likelihood (ML) and Maximum Parsimony (MP).

All sequences used in both analyses have been functionally and/or phylogenetically characterized in previous works; for six of them crystal structures are available. Two trees were generated through the MEGA7 program (33); the first one was made with the ML method, with 100 bootstrap replicates and the second tree was obtained with the MP method again with 100 bootstrap replicates. The alignment of the protein sequences and key amino acids were analysed using the Jalview 2.9.0b2 software. The levels of amino acid conservation in photoreceptors were drawn using WebLogo (http://weblogo.berkeley.edu/logo.cgi).

Three dimensional modeling. A comparative modeling technique was used to obtain three-dimensional models of HAAL's extremo-photoreceptors. First, PSI-BLAST was used to search the database for modelling templates (44) in the Protein Data Bank (PDB, www.pdb.org). The structures employed as models are listed in Table 2. The sequences were then aligned manually to adjust the models and finally 100 3D models were obtained per protein, using the software Modeller 9.14 (45). The models with the lowest score were selected according to DOPE score (Discrete Optimized Protein Energy), which is used to evaluate the energy of the model generated by Modeller 9.14. This selection identifies the lower DOPE score with lower free energy associated with the model, and is taken as criterion for the best model for the protein of interest.

Energetic and structural analyses were carried out to assay the quality of the chosen models. In the beginning, we obtained the DOPE profile (with modeller by Phyton) for the sequence of amino acids in the 3D structure, both for the model and for the template, for each CPF member. Then we generated a graph with the two DOPE profiles for the selected model and the template employed in order to determine the similarity between model and template. The Ramachandran graphics were also generated in the MolProbity server (46), which

provides an easy way to evaluate the distribution of the torsion angles of a protein structure, and also provides an overview of the allowed and not allowed regions, which serves as an important indicator of the quality of the three-dimensional structure of a protein. Also, the Z-scores and the energy were determined according to the position in the sequence of the models through the ProSA server (47), which allows determination of the quality of the general model and comparison of its score with the score of proteins crystallized by X-rays or NMR of similar sizes. The energy analysis along the sequence allows detecting regions with positive energy that are usually problematic or carry errors.

RESULTS AND DISCUSSION

UV-B resistance profile

UV resistance profiles of the studied strains and their respective controls indicated that HAAL's poly-extremophiles were much more resistant to radiation than phylogenetically related bacteria used as control strains (**Fig. 2A-C**). *Acinetobacter* sp. Ver3 (herein, Ver3) was the most tolerant strain within the *Acinetobacter spp.* strains tested, being able to grow up to a UV-B dose of 42 kJ m^{-2} (240 min), while *A. johnsonii* DSM 6963 (AJ), *A. baumannii* DSM 30007 (AB) and *A. lwoffi* DSM 2463 (AL) showed a clear inhibition even at lower exposure times (**Fig. 2A**). These results agreed with previous findings for the *Acinetobacter* sp. Strains (19,39).

The poly-extremophilic actinobacterium *Nesterenkonia* sp. Act20 (21) (herein, Act20) was able to endure higher UV-B irradiation (UV-B dose: 68 kJ m^{-2}) than Ver3 and *Exiguobacterium* sp. S17 (herein, S17). Act20 showed a relative survival of 70 % after 68 kJ UV-B irradiation, whereas *N. halotolerans* DMS 15474 (NH) showed a relative survival of

only 20% (**Fig. 2C**). S17 was able to grow up to the maximum dose tested (120 m, UV-B dose: 38.8 kJ m^{-2}) while *E. aurantiacum* (EA) was completely inhibited after 90 min of exposure (**Fig. 2B**).

The superior UV resistance ability of HAAL strains indicate a clear adaptation to high radiation exposure encountered in their original habitat (1), which otherwise have selected a multifaceted system of shared genetic and physiological mechanisms called as UV-resistome (37). Thus, the UV-resistome depends on the expression of a diverse set of genes devoted to evade or repair the damage provoked direct or indirectly (2). Following this assumption, we compared Ver3, Act20 and S17 gene determinants involved in the following sub-systems: 1- UV avoidance and protection strategies; 2- Stress sensors with their corresponding response regulators; 3- Damage tolerance and oxidative stress response; and 4- DNA damage repair (**Supplementary File S2**). From the three strains, Act20 genome showed the most diversified response to UV as all subsystems proposed were found; this in agreement with its higher resistance profile to UV.

From all the subsystems found, we herein characterize more in detail photoreactivation abilities (included in the subsystem of DNA damage repair) and pigment content (included in the subsystem of UV avoidance and protection strategies) in the selected HAAL strains.

Photorepair ability

To evaluate if photoreactivation is involved in the UV-resistance mechanism of HAAL's strains, their photorepair ability was tested in comparison with the sensitive controls (**Fig. 2D-F**). Selected strains were first exposed to UV-radiation: 6.4 kJ m^{-2} for Ver3, 9.7 kJ m^{-2} for S17, and 12.9 kJ m^{-2} for Act20. In these conditions, Ver3 and AL demonstrated a relative survival of 40 %, in contrast to AJ and AB that showed a relative survival of only 2

and 10 %, respectively (**Fig. 2D**). Aliquots of the UV-B challenged cells were then subjected to photo repair (PR) or dark repair (DR). After PR treatment, all strains increased their survival substantially. Ver3 showed the highest photoactivation ability among all *Acinetobacter* strains, reaching values of up to 80 %, followed by AL(50 %), AJ(20%) and AB(<10%).

The resistance/photorepair profile was quite different for S17 and EA; after UV-B treatment, S17 was able to grow until a 64 %, and then it recovered with values of 77 % for DR and 87 % for PR, while UV-B exposed EA showed a 7 % survival without recovering its viability after both, DR or PR (**Fig. 2E**).

Act20 and NH showed a 52% and 40% of survival after UV-B exposure, respectively. When exposed to the repairing treatments, they completely recovered under PR, and showed 67% (NH) and 79% (Act20) of viability after DR (**Fig. 2F**). This was in line with our expectations, since both *Nesterenkonia* strains were isolated from arid environments with high UV exposure (21,48,49).

Irrespective of the strain tested, photorepair was the most effective treatment to increase survival after UV-B. This phenomenon may be explained by the synergic effect of photolyase activity together with all repair mechanisms independent of light activation such as NER (Nucleotide excision repair). In fact, it was suggested that photolyases can participate in light-independent repair (50,51); *E. coli* and yeast photolyase activities enhanced dark survival via specific stimulation of excision repair (50,52). Sancar et al. (1984) (51) have shown that binding of photolyase to pyrimidine dimers enhances the recognition of dimers by the excision nuclease.

Similar UV-resistance profiles were found for other microbes or microbial communities reported in the HAAL; Ordoñez et al (2009) (35) isolated and characterized HAAL's UV-B resistant bacteria from six Andean lakes belonging to proteobacteria,

Cytophaga-Flavobacterium-Bacteroides group, Firmicutes, Actinobacteria and *Bacillus.* Fernandez Zenoff et al. (2006) (53) studied the UV-B resistance of the culturable bacterial community from high-altitude wetlands; among all strains, the actinobacterium A5 was able to survive doses of 3201 kJm^{-2} under an irradiance of 4.94 W/m^2. Flores et al. showed in 2009 (17) that Andean lakes bacterial communities were well adapted to high UV-B exposure and in many cases UV-B even stimulated their growth.

.

Pigment content

Light may damage biological systems by causing the excitation of photosensitive molecules (i.e. a sensitizer) which could initiate potentially harmful photochemical reactions with the surrounding molecules to generate highly reactive free radicals (101). Among the resources that microorganisms display to protect themselves from light, carotenoids are effective photo-protective compounds widespread in prokaryotes and eukaryote organisms (103). Carotenoids are diversified pigments ranging from red to yellow and produced by a wide variety of bacteria, algae, fungi, and plants. These poly-isoprenoid compounds can be divided into two main groups: (i) carotenes or hydrocarbon carotenoids, which are composed of carbon and hydrogen atoms, and (ii) xanthophylls that are oxygenated hydrocarbon derivatives that contain at least one oxygen function such as hydroxyl, keto, epoxy, methoxy, or carboxylic acid groups (54). The protective action of carotenoids against photodynamic effects is related to their range of light-absorption and their antioxidant properties in both photosynthetic and non-photosynthetic organisms (49). Thus, in order to determine the involvement of carotenoids on the UV-B resistance profiles of the tested strains, pigment extractions were performed followed by a spectrometric analysis (**Fig. 3**).

The extract of *Acinetobacter* sp. Ver3 did not present peaks of absorption in the range of the visible light indicating the lack of pigments, while the smallest peak at 280 nm may be due to the absorption of the solvent used (**Fig. 3**). This evidence is in line with the whitish, almost transparent aspect of Ver3 cells and with the lack of carotenoids-coding genes in Ver3 genome (Supplementary File S2). Therefore, we suggest that pigment protection and/or ROS quenching by pigments is not involved in the high UV-B resistance of Ver3. In turn, both, the yellowish extract of *Nesterenkonia* sp. Act20 and the orange extract of *Exiguobacterium* sp. S17 shows a carotenoid-like absorbance spectrum (49), with maximum absorbance at 434 nm and 466 nm, respectively. For comparison, we have included three different pigment spectra; spectra from HAAL strains are more similar to the B-carotene control. Accordingly, genes involved in carotene biosynthesis where found in Act20 and S17 genomes (**Supplementary File S2)**. Previous works indicated that *Exiguobacterium aurantiacum* FH, a strain isolated from air, produced carotenoids (carotenes and xanthophylls) that displayed antifungal activity (Shatila et al., 2013). In turn, this is the first report of carotenoid pigments produced by a *Nesterenkonia* strain.

Interestingly, S17 shows a clear absorbance in the 275-300 range, with peaks of significant intensity at 285 and 277 nm with a shoulder at 300 nm. These peaks could be explained as a second pigment able to absorb light in the UV-B range, i.e., such as the carotenoid 15-cis-4,4'-diapophytoene of *Staphylococcus aureus* (52). An alternative explanation is that the peak at 287 nm is due to the absorbance of an intermediate compound of the synthesis of the carotenoid absorbing at 466 nm; Tao and Cheng studied the synthesis of a canthaxanthin from *Rhodococcus erythropolis* (50), and shows that the intermediate compound lacking the 4-keto group, the phytoene backbone, has a maximum absorption peak at 286 nm, while the insertion of the keto group to form 4-ketoγ-carotene did not absorb at 286 but has it maximum at 450 nm.

The function of carotenoids in biological systems and their contribution to light stress has been largely studied (102). Carotenoids are considered to protect microorganisms, animals and plants from the destructive effects of activated oxygen species, such as superoxide (O_2-), hydrogen peroxide (H_2O_2), singlet oxygen ($1O_2$) and hydroxy radical (OH), and are known to quench $1O_2$ (Tatsuzawa 2000). Many works reported positive effects of carotenoids and related them with UV-B protection in bacteria (54–57). It was mentioned that UV-B may have an indirect damage effect by promoting the formation of reactive oxygen species (ROS), which are highly toxic; likewise, UV-B can directly affect biomolecules like lipids, proteins, and DNA by photolysis (Das 2014). The ROS plays the double role of being the inevitable by-product of aerobic metabolism on one hand and serving as a marker during stressful conditions on the other hand. The ROS defense mechanism consists of the antioxidant machinery which helps to mitigate the above mentioned oxidative stress-induced damages. The antioxidant machinery has two arms with the enzymatic components and non-enzymatic antioxidants. The machinery enzymatic includes Superoxide Dismutase (SOD), Catalase (CAT), Ascorbate Peroxidase (APX), Monodehydroascorbate reductase (MDHAR), Dehydroascorbate reductase (DHAR), Glutathione Reductase (GR), and Guaiacol Peroxidase (GPX). While the non-enzymatic antioxidants comprising of acid ascorbic (AA), reduced glutathione (GSH), α-tocopherol, carotenoids, phenolics, flavonoids, and amino acid cum osmolyte proline (Das 2014). Most of these proteins or metabolic pathways are presented in the annotated genome of Ver3, S17 and Act20 (**Supplementary File S2**). In addition, *Acinetobacter* sp. Ver3 demonstrated efficient ROS scavenging systems as a response to UV-B exposure (Di Capua et al., 2012; Kurth et al., 2015). Further studies using functional genomics are in progress to characterize and integrate all the mechanisms of UV-protection/ROS quenching in the HAAL's strains.

Singh et al. (2011) (58) highlighted the importance of studying UV-resistant microbes and their metabolites as source for potential therapeutics. Some examples are: (i) the mycosporine-like amino acids (MAAs) acting as a 'sunscreen' for UV radiation in the wavelength range 310–365 nm (59) are found in a wide range of micro-organisms including cyanobacteria and eukaryotic algae and protect against UV-induced DNA damage by preventing the formation of DNA dimers. They are already used as one of the compounds in UV sunscreens in the cosmetics industry, and have been suggested for potential applications in the prevention of skin cancer induced by UV-radiation such as melanoma (60). (ii) Scytonemin is a secondary metabolite and an extracellular matrix (sheath) pigment synthesized by many strains of cyanobacteria (61). It is an aromatic indole alkaloid built from two identical condensation products of tryptophanyl- and tyrosyl-derived subunits linked through a carbon-carbon bond (62,63). It could act as a highly efficient protective biomolecule (sunscreen) that filters out damaging high frequency UV rays while at the same time allowing the transmittance of wavelengths necessary for photosynthesis (64). (iii) Ectoine is a small organic molecule, present widely in aerobic, chemoheterotrophic and halophilic organisms. These organisms protect their biopolymers against dehydration caused by high solar exposure, high temperature, salt concentration and low water activity. Halophilic microorganisms synthesize ectoine from aspartate semialdehyde in three steps. Ectoine is already employed as protectant for human skin, in a number of different ways to avoid UV-A induced cell damage; In fact, Lentzen and Schwarz in 2006 (65) could produce ectoine by a continuous fermentation of *H. elongate*. (iv) Bacterioruberin, a C_{50} carotenoid pigment present within the membrane of many radioactivity-resistant microorganism, as *H. salinarum*. The primary role of bacterioruberin in the cell is to protect against DNA damage

incurred by UV light (66). Bacterioruberin protects the DNA by acting as an antioxidant, rather than directly blocking UV light. It is able to protect the cell from reactive oxygen species (67).

Genome screening for cryptochromes and photolyases

Considering the experimental proof of efficient photorepairing in HAAL's strains, genomes were screened for the presence of sequences with homology to known photolyases/cryptochromes (**Table 1**). Each of the three genomes displays at least one classical photolyase and one cryptochrome clustering together with the so-called FeS-BCPs group. FeS-BCPs comprehend a newly characterized CPF members containing the amino acids necessary to bind the cofactors, and in addition four conserved cysteine residues for the coordination of an iron-sulfur cluster (32).

Acinetobacter sp. Ver3 presents two CPF sequences: Ver3Phr, a photolyase class I showing 67% identity with the photolyase from *Acinetobacter* sp. VT 114 (WP_054581756) (68) and Ver3Cry, a putative cryptochrome displaying 95**%** identity with a cryptochrome from *Acinetobacter* sp. VT 511 (WP_048881868). The latter protein can be classified according to Geisselbrecht (2012) (69) as a member of the new clade Cry-Pro. These cryptochromes are usually present in proteobacteria and cyanobacteria. The cryptochrome B (CryB) from *Rhodobacter sphaeroides* has been characterized and the crystal structure is already available. It is involved in the regulation of photosynthesis gene expression (69). The Cry-Pro were classified in a wider clade of proteins called as FeS-BCP, with 350 sequences identified from bacterial organisms, and also including many human and plant pathogens such as *V. cholera* and *P. syringae* (32). Zhang et. al. (2013) (70) and Zadow et al. (2016) (71) also described photolyase (6-4) activity for a FeS-BCP sequence from *A. tumefaciens* and *Rhodobacter sphaeroides*.

The genome of *Exiguobacterium* sp. S17 revealed the presence of three proteins belonging to the CPF family: (i) S17Phr, a putative CPD-Class I photolyase displaying 83% identity with other photolyases from *Exiguobacterium mexicanum* (WP_034777040); (ii) S17Cry, a putative cryptochrome FeS-BCP with identity of 84 % with a CPF of *Exiguobacterium pavilionensis* (WP_021066163), and (iii) S17CryD, a putative Cry-DASH with 79 % identity with a Cry-DASH from *Exiguobacterium alkaliphilum* (WP_034817977). Cry-DASH is a subgroup of the Cry gene family, which name indicated the taxa in which it was originally reported i.e. *Drosophila, Arabidopsis, Synechocystis*, and *Homo* (72). Nevertheless, it was later described to be present innon-photosynthetic bacteria, fungi, plants and animals, including *Neurospora*, zebrafish and *Xenopus*. Both, structural and functional studies suggest that Cry-DASH proteins function as transcriptional repressors in *Arabidopsis* and *Synechocystis* (73,74). However, Selby and Sancar (2006) have demonstrated that the *Arabidopsis* At-Cry3 and other Cry-DASH exhibited single-stranded DNA photolyase activity.

In turn, *Nesterenkonia* sp. Act20 presents two sequence homologues to CPF in its genome: (i) Act20Phr, a putative CPD- Class III photolyase with 83% identity with a CPD from *Nesterenkonia* sp. AN1 (WP_036475602), and (ii) Act20Cry,a putative cryptochrome FeS-BCP with an identity of 75% with a CPF of *Nesterenkonia* sp. AN1 (WP_036477144). Up to now, only one crystal structure of the type CPD class III photolyases is available and was reported for *Agrobacterium tumefaciens* (75**).** Within the *Nesterenkonia* genus, no specify studies on photoreceptors were reported and therefore, little is known about their biological mechanisms, which otherwise does allow these microbes to survive in their original hostile environment.

Conserved domains and functional residues of photolyases and cryptochromes

Inspection of protein sequences of putative CPD-photolyases Ver3Phr, S17Phr and Act20Phr showed two clear domains: pfam03441 FAD binding domain of DNA photolyase and pfam00875, specific of DNA photolyases, which binds a light harvesting cofactor. In Act20Phr, an even more conserved zone was identified within the domain pfam00875, a region cd00293 called Usp (universal stress protein family). Usp is a small cytoplasmic bacterial protein whose expression is enhanced when the cell is exposed to stress agents.

In turn, the three putative cryptochromes of the FeS-BCP clade Ver3Cry, S17Cry, and Act20Cry showed a single conserved N-terminal domain: pfam04244 being member of the superfamily cl04458 (Deoxyribodipyrimidine photolyase-related protein). S17CryD presents the typical Cry-DASH domain TIGR02765 together with the two domains already described as pfam03441 and pfam00875.

Multiple sequence alignments (MSA) among HAAL's photolyases and cryptochromes in comparison with reference sequences (**Fig. 4A and 5A**) allow us to confirm the conserved regions and key residues involved in functional activity: i.e. FAD binding (Phr/Cry), it was also searched the specific amino acids such as W-triad (Phr) and specific residues for the union of other cofactors such as FeS cluster binding (Cry) which help us for the classification. A better way to evidence the levels of amino acid conservation is by drawing a sequence logo (seqLogo) from an MSA (**Fig. 4B and 5B**). The produced cartoon displays statistically significant differences in position-specific symbol compositions among multiple sequence alignments (76). In addition, we obtained one-hundred models for each HAAL's photoreceptor to assess structural similarity with homologue crystalized proteins. Models with the lowest DOPEs-scores were selected for each photoreceptor (**Fig. 6**). The DOPE profile was calculated for both, templates and models, and represented in a plot as a fast way to compare their similarity. For all seven cases, the DOPE profile of the model show the same

pattern as the template. The Ramanchandran plot also showed a good folding of the models (**Supplementary Files S3-S9**). The Z-score and the energy profile per amino acid residue were determined as another way to evaluate the quality of the models, comparing them with crystallized structures (Table 2). For all models, the values of Z-score were similar to the template and always fitted between the maximum and minimum values.

The activity of proteins from the CPF family depends on the possibility of changing the oxidation state of the bound FAD, allowing a cycle reduced-oxidized-reduced, which is favored by the generation of an excited initial state caused by UV-A (320–400 nm) and blue light (400–500 nm). This oxidation state cycle generates the repair activity on the damaged DNA in the case of the photolyases, and for the cryptochromes it is considered as the starting event for the signaling cascade (77). Thus, we analyzed in all HAAL's photoreceptors the N-terminal region, responsible of the FAD binding in the MSA (**Fig. 4**) and 3D models (**Fig. 6-7 and Supplementary Files S3-S9**). Overlays of the photolyases Ver3Phr, S17Phr and Act20Phr against templates show a good structural similarity that materializes in a congruent fold of the protein (**Fig. 6 and Supplementary files S3, S5 and S8**). The structures revealed a α/β domain in the N-terminal region and a second α helix domain in the C-terminal region, both connected by a long inter-domain loop that envelops the α / β domain as it is common in photolyase. The α / β domain showed a Rossman fold with five parallel β strands covered at its sides by α helices, which also is seen in other photolyases. The binding site for FAD in photolyase of *E. coli* (EcPhr) is composed by the following residues: Y222, T234, S235, R236, L237, S238, Q239, W271, T338, N341, R344, D372, D374, and N378 (19**).** These conserved sites in *E. coli* correspond in Ver3Phr to Y225, T237, S238, L240, S241, W276, R283, W343, N346, D377, D379 and R236. In S17Phr, the corresponding amino acids are Y215, T227, S228, L230, S231, W326, N329, N366, R332 and D360. In Act20Phr, the

amino acids Y235, T247, S248, L250, S251, H348, N351, N388, R354 and D382 are identified as the binding site components**.**

Photoactivation is a key step in the photolyases action mechanism, leading to the reduction of FADH° to FADH-; it was reported that FADH° is reduced within 1 ms by intra-protein electron transfer from W306 in *E. coli* Phr (78). W306 is part of the tryptophan-triad (W-triad) which is well studied in the photolyase from *E. coli* (W306, W359 and W382) (75). This triad is highly conserved in most characterized photolyases, including Cry-DASH proteins which use the W-triad to repair single stranded DNA (72). In HAAL's photoreceptors, the W-triad is conserved for the photolyases and S17CryD (**Fig. 4A and 4B**), while it is absent in the putative FeS-BCP cryptochromes **(Fig. 5A and 5B)**, which raise the question whether these cryptochromes exhibit repair activity. Although, the absence of the triad does not rule out the possibility of photo repair as it was proved that an *E. coli* photolyase carrying mutations in the W- triad is still active *in vivo* (26). Furthermore, Tyr residues are also involved in ET in other photolyases: e.g. in the CPD class I photolyase from *Anacystis nidulans* (78) (Aubert 1999) and in *Methanosarcina mazei* CPD class II photolyase, a Tyr residue is required for full photoreduction. In the *Xenopus laevis* (6–4) photolyase the involvement of a Tyr residue in photoreduction was shown by electron paramagnetic resonance (79,80) (Weber 2002, Holub 2017). But in all cases studied the tyrosine are coupled to tryptophans. The W-triad in Ver3Phr is W286, W363, and W310 (81), in S17Phr it is W369, W346, and W293, in Act20Phr it is W391, W368, and W312, and in S17CryD it is W369, W345, and W292 (**Fig. 4A and Fig. 8A-C)**. The 3D models confirm the presence of the W-triad, which aligned coincidently in all three Phr models (**Fig. 8A**).

In addition, the binding site for the second cofactor is characteristic in some photolyases, and the amino acids are merely conserved, as shown in the sequence alignment around the positions of N108, E109, C292, and K29 (**Fig. 4A**). The CPD class I of Ver3 is

the most similar to the CPD of *E. coli* in the amino acids sequence binding a second cofactor. The second cofactor in *E. coli* photolyase is MTHF, and glutamic acid is key for MTHF binding (82,83) (Muller 2009).

For the FeS-BCPs, the region containing the four cysteines for the sulfur part of the cluster (4Fe4S) (69) is the most conserved part (**Fig. 5B**); in *Rhodobacter sphaeroides* they were identified as C346, C434, C437 and C45069. In the MSA, these residues are conserved in Ver3Cry and S17Cry but lost in Act20Cry **(Fig. 5A**). In coincidence, when an overlay is performed for the BCP-FeS putative sequences (**Fig. 7D-F**), the four Cysteines are conserved and coincident in their spatial distribution, with the only exception of Act20Cry, which shows at the corresponding positions two proline (C381, C470), one alanine (C476) and one aspartate residue (C473). It is accepted that the cysteines are necessary to coordinate the [4Fe-4S] cluster of the large subunit of primases (PriL-CTD) in archaea and eukarya and in FeS-BCPs (32,69). The absence of the pattern may indicate a loss of [4Fe-4S] cluster, a novel function or/and a different structural disposition of the Act20Cry. Nevertheless, there are some examples where the clusters are bound or established for other amino acids different than cysteines (84). Robyn et al. (2006) (85) studied biotin synthase, an enzyme that catalyzes the addition of sulfur to dethiobiotin that contains a cluster of 4Fe4S, in this work they detail that the cluster is stabilized by the three cysteines and an arginine, this last one is fundamental for maintaining the activity of the proteins. In Zu 2003 (86) they analyze and cite more than one example of proteins called Rieske [2Fe-2S] clusters, where the cluster is stabilized by two histidine residues. However, there is no evidence for a cluster [Fe-S] without the stabilizing four cysteinesin FeS-BCP cryptochromes -they are strictly conserved in crystallographic structures and widely retained in the clade- suggesting a low chance to find a cluster [Fe-S] coordination in the Act20Cry product. Interestingly, phylogenetic analysis indicated that the Act20Cry protein clustered in the FeS-BCP closer to the root and

quite distant from the other members including Ver3Cry, S17Cry and the readily characterized FeS-BCP from *A. tumefasciens* and *R. sphaeroides* **(Fig. 8).**

On the other hand, the function of the FeS cluster is not very clear yet; usually the [4Fe-4S] clusters are oxidized acting as sensor for reactive oxygen species. Then, oxidative damage of the cluster could trigger disordering or structural change of the C-terminal end and alter the DNA binding, which in turn can act as a photoreactive agent, in a similar way to that proposed to the W-triad (69). This hypothesis may be sustained as FeS-BCP from *Rhodobacter sphaeroides* showed [6-4] photolyase activity (71); this kind of proteins had initially been thought to be absent in prokaryotes and in most eukaryotic organisms (70,71). Photolyase-like genes with Fe-S clusters were confirmed in the two strains of HAAL analyzed in this article, suggesting a possible [6-4] photolyase activity for them. The formation of the [6-4] photoproduct depends on the dose of UV radiation and increases with increasing dose reaching up to 40% of the photoproduct fraction (28). It is likely that the acquisition of [6-4] photolyases by HAAL bacteria is a compensatory adaptation to the high dose of UV radiation present in their original environment. However, in HAAL's *Acinetobacter* strains the most common photoproducts repaired were the cyclobutane pyrimidine dimers (CPDs) (19). For further characterizations, assessment of a repair function for (6-4) photoproducts will be needed in these strains. Other possible functions of these cryptic photoreceptors may be to stimulate the NER system or to act as regulators enhancing photoreactivation or stress recovery upon UV-B. In previous work, a FeS-BCP has been reported to act as a cryptochrome regulating the expression of the photosynthetic apparatus in *Rhodobacter sphaeroides* (69). Although the herein selected HAAL's bacteria are not photosynthetic, the abundance and quality of sunlight available in the Andean lakes, as well

as the molecular versatility of this family of proteins, provide the microorganisms harboring them an advantage in an extreme environment where energy and nutritional resources are scarce.

Phylogeny of bacterial photolyases and cryptochromes

The phylogenetic analysis was designed in order to compare the HAAL's sequences with homolog bacterial proteins with documented functional or structural information (**Fig. 8A)**. The sequences clustered into eight groups; six of them were previously described as CPD class I photolyases (type 8-HDF), CPD class I photolyases (type MTHF), CPD class II photolyases, CPD class III photolyases, Cry-DASH and FeS-BCP-cryptochromes (34). Furthermore, two additional groups were identified herein: they include the sequences of *Thermus thermofilus* HB27 and *Streptomyces griseus*, respectively. A similar outcome was found when ca. 100 sequences from the database were added to the analysis (**Supplementary File S10-S12**).

The photolyase from *Thermus thermophilus* HB27 (87) resides at a debatable phylogenetic position. In some works, it is included in the CPD class I photolyases (69,75,88,89), while in others lies in different clusters (32,90,91). It is stable at temperatures over 60 ºC and presents flavin mononucleotide (FMN), a highly efficient (92) second chromophore that has not been found in other bacterial CPD photolyases. The genus *Thermus* sp. usually reaches its optimum living temperature between 65 ºC and 72 ºC (93), making it an excellent source of extremozymes. The closest orthologous photolyase in the databases belongs to the genus *Meiothermus* sp., which is also a thermophile with an optimal temperature range between 50 ºC and 65 ºC (94). However, there is no functional proof or analysis reported, that this protein intervene in the photo-reactivation process.

The photolyase of the genus *Streptomyces* sp., functionally characterized only in *Streptomyces griseus*, has been included in previous works as a member of CPD class I photolyases with an unidentified antenna cofactor, possibly derived from 8-HDF (8-hydroxy-7,8-didemethyl-5-deazariboflavin) (95–97). The genus *Streptomyces* is known for its remarkable biological, metabolic and genetic complexity as they showed the most complex biology growing with branched mycelium, filaments with hyphae and reproducing aerial branches with chains of spores (98); in this way, a good part of its biological cycle is exposed to radiation. In addition, they are producers of the largest number of antibiotics, 8,700 antibiotics estimated in 2002, compared to 2,900 produced by the rest of the bacteria, and 4,900 by fungi (99), as well as generators of a variety of enzymes for extracellular digestion and signaling molecules. In agreement, with its complex life style and metabolism, they allocate large genomes (8-9 Mb, approximately), with the highest estimated number of genes (100). As members of the phylum Actinobacteria, *Streptomyces* display a large G-C content in this genome, mostly above 70% unlike other Gram-positive bacteria whose G-C content is usually less than 50%. It should be kept in mind that the higher the G-C content, the lower is the amount of total photoproduct, although an increase of photoproduct with cytosine content is observed, which is highly mutagenic compared to the photoproduct TT (101,102). These characteristics make their genomes more exposed to photo inducible mutations. Some of these traits are also found in other genera of Actinobacteria (100). It is probable that some of these factors or the combination of more than one have influenced the notable specialization of the enzyme photolyase resulting in a separated clade (**Fig. 8**).

To trace the evolution of the family BCP, a phylogenetic analysis was performed using both, Maximum Likelihood (ML) and Maximum Parsimony (MP) methods. They were plotted using cladograms **(Fig. 8B and 8C)** in order to identify the main steps of molecular

evolution in the CPF family in bacteria. For our knowledge, this is the first analyses of CPF evolutionary process taking in account only the bacterial domain.

The main steps in the evolution of groups of bacterial photolyases are presented (**Fig. 8B and 8C)**. The first photolyase described *(step 1)* would have resulted from the duplication of a gene with an [Fe/S] cluster that acquired the function of CPD repair (70). The gain of an antenna *(step 2)* in order to amplify the energy absorption would be the next step. This chromophore would probably have been flavin itself or a derivative (8-HDF, FMN, DMRL, FAD) for several reasons. Among others one would consider its high photochemical efficiency, required in a primitive environment without a protective atmosphere against UV rays (95,97). The change *(step 3)* of the CPD function by [6-4] repair would result in the FeS-BCP class or photolyases and bacterial cryptochromes with iron-sulfur cluster. The early appearance of this function would increase the amount of photoreactivation, considering that the photoproduct [6-4] is abundant at high doses of UV irradiation (28), characteristic of the environment in which prokaryotes evolved. The loss of the cluster [Fe/S] *(step 4)* would have been the following step for the origin of the majority of the current members of the family. A long deletion *(step 5)* in the C-terminal α helix domain, which affects the FAD binding mechanism, may give rise to the CPD II photolyases (97,103). Photolyases CPD class III *(step 6)* would have originated from the recruitment of the pterinic chromophore (MTHF), which, although less efficient, is more abundant in nature (83,94,95). This class of photolyases includes an alternative photoreactive triad and the stabilization of the MTHF chromophore by π-stacking. Other recruitments of the MTHF,yet in a different and poorly conserved site would have occurred in folate CPD I *(step 7)* and some Cry-DASH proteins *(step 8).*

Concluding remarks

In this work, we compared the UV resistance profiles, pigment content and photoreactivation abilities of three UV-resistant bacteria isolated from distinct niches from HAAL's; out of these, the soil actinobacterium, *Nesterenkonia* sp. Act20, was found to be the most resistant extremophile.

UV resistance ability of HAAL's strains indicate a clear adaptation to high radiation exposure encountered in their original habitat, which can be explained by genetic and physiological mechanisms called as UV-resistome. Thus, the UV-resistome depends on the expression of a diverse set of genes devoted to evading (pigments, wall components, biofilm formation) or repairing/coping the provoked damage (DNA repair/oxidative stress response) which are currently under further investigation by multi-omics approaches.

Two components of the UV-B resistome were further explored in this paper; pigment extraction indicate the presence of carotenoid-like compounds in S17 and Act20 cells suggesting an antioxidative defense or protective role for them. On the other hand, photoreactivation upon UV-B damage was efficient in all three strains; consequently, we found proteins with homology to photolyases/cryptochromes (CPF) in Ver3, Act20 and S17 genomes. Each one displays at least one classical photolyase and a cryptochrome clustering together with the so-called FeS-BCPs group. Phylogenetic analyses, sequence comparison and 3D modeling with bona fide CPFs were used to proof the presence of functional domains (FAD binding) and key residues (W-triad) in the novel proteins. The most intriguing protein was, however, Act20Cry for which the phylogenetic analyses indicate a close relation with BCPs carrying an iron-sulfur cluster. However, so far inspection of the sequence in detail and 3D homology models suggests no possible cluster coordination for this protein. Further overexpression, purification and spectroscopic/structural characterization of Act20Cry will be needed to solve this open question.

SUPPORTING INFORMATION

Additional supporting information is available in the Supporting Information section at the end of this article:

Supplementary File S1. UV-B lamp and acetate filter spectra.

Supplementary File S2. UV-resistome components found in HAAL strains.

Supplementary File S3. Modelling and quality evaluation of Ver3Phr. **A.** Ver3Phr Model; **B.** Superposition of model and template; **C.** DOPE-profile plot; **D.** Ramachandran plot; **E.** Z-score plot; **F.** Energy-profile plot.

Supplementary File S4. Modelling and quality evaluation of Ver3Cry. **A.** Ver3Cry Model; **B.** Superposition of model and template; **C.** DOPE-profile plot; **D.** Ramachandran plot; **E.** Z-score plot; **F.** Energy-profile plot.

Supplementary File S5. Modelling and quality evaluation of S17Phr; **A.** S17Phr Model; **B.** Superposition of model and template; **C.** DOPE-profile plot; **D.** Ramachandran plot; **E.** Z-score plot; **F.** Energy-profile plot.

Supplementary File S6. Modelling and quality evaluation of S17CryD **A.** S17CryD Model; **B.** Superposition of model and template; **C.** DOPE-profile plot; **D.** Ramachandran plot; **E.** Z-score plot; **F.** Energy-profile plot.

Supplementary File S7. Modelling and quality evaluation S17Cry; **A.** S17Cry Model*;* **B.** Superposition of model and template; **C.** DOPE-profile plot; **D.** Ramachandran plot; **E.** Z-score plot; **F.** Energy-profile plot.

Supplementary File S8. Modelling and quality evaluation ofAct20Phr; **A.** Act20Phr Model; **B.** Superposition of model and template; **C.** DOPE-profile plot; **D.** Ramachandran plot; **E.** Z-score plot; **F.** Energy-profile plot.

Supplementary File S9. Modelling and quality evaluation Act20Cry. **A.** Act20Cry Model; **B.** Superposition of model and template; **C.** DOPE-profile plot; **D.** Ramachandran plot; **E.** Z-score plot; **F.** Energy-profile plot.

Supplementary File S10. Phylogenetic tree of Cryptochrome/Photolyase family members of the Bacteria domain generated using neighbor joining methods. Eight classes are identified, including two new groups: BCP-FeS (brown), Class II CPD photolyase (pink), Cry-DASH (purple), 8-HDF type class I CPD photolyase (red), MTHF type class I CPD photolyase (blue), Thermus related photolyase (orange), Streptomyces related photolyase (green) and Class III CPD photolyase (cyan). Photolyases with a certain level of confidence fall into 6 groups: photolyases with crystal structures (a), functionally expressed and characterized product (b), sequence characterized (c), function confirmed (d), function inferred by photoreactivation assays (e) and inferred by homology (f). These sequences including the seven putative photolyase and cryptochrome sequences from *Acinetobacter* sp. Ver3, *Exiguobacterium* sp. S17 and *Nesterenkonia* sp. Act20 are in bold and large print. Red dots represent nodes with a >50% bootstrap value. Schemes of evolutionary process for the photolyase-cryptochrome family with **B.** Maximum Likelihood and **C.** Maximum Parsimony methods. Bootstrap values are shown in the trees and each step is explained in the text.

Supplementary File S11. List of sequences used to build main phylogenetic tree.

Supplementary File S12. List of sequences used to build supplementary phylogenetic tree.

Supplementary File S13. Absorbance spectrum of standard pigments.

ACKNOWLEDGEMENTS

The authors acknowledge the generous financial support by the PICT V Bicentenario 2010 1788, PICT 2013 2991 Projects (FONCyT, Argentina) and PIP CONICET 0519 Project. V.H.A. was supported by a Marie Curie FP7-People-2010-IIF EXTREMOPHIL(273831) in Germany and its return phase in Argentina (PIIFR-GA-2010-910831-EXTREMOPHIL). MEF, VHA and MV are researchers from the National Research Council (CONICET) in Argentina. LP, FZ and DA are recipients of fellowships from CONICET. Electron micrographs used in this study were taken at the Research Center for Electron Microscopy and Core Facility (CIME) belonging to UNT and CCT, CONICET, Tucuman.

REFERENCES

1. Albarracín, V. H., D.Kurth, O. F. Ordoñez, C. Belfiore, E. Luccini, G.M. Salum, R. D. Piacentini and M. E. Farías (2015) High-Up: A Remote Reservoir of Microbial Extremophiles in Central Andean Wetlands. *Front. Microbiol*. 6:1404.

2. Albarracín, V. H., W. Gärtner and M. E. Farias (2016) Forged Under the Sun: Life and Art of Extremophiles from Andean Lakes. *Photochem Photobiol*, 92: 14–28.

3. Duffie, J. A. and W. A. Beckman (2013) Solar Engineering of Thermal Processes. Hoboken, N J: JohnWileyand Sons, Inc.

4. Escudero, L., G. Chong and C. Demergasso (2007) Investigating microbial diversity and UV radiation impact at the high-altitude Lake Aguas Calientes, Chile. *Instruments, Methods, and Missions for Astrobiology X*; 66940Z.

5. Piacentini, R. D., A. Cede and H. Bárcena (2003) Extreme solar total and UV irradiances due to cloud effect measured near the summer solstice at the high-altitude desertic plateau Puna of Atacama (Argentina). *J Atmos Solar-Terrestrial Phys.* 65(6):727-731.

6. Piacentini R. D., A. Cede, E. Luccini and F. Stengel (2004) Determination of the UV solar risk in Argentina with high-resolution maps calculated using TOMS ozone climatology. *Adv Sp Res.* 34(10):2215-2220.

7. Luccini, E., A.Cede, R. Piacentini, C. Villanueva and P.Canziani (2006) Ultraviolet climatology over Argentina. *J Geophys Res.*111(D17):D17312.

8. Cabrol, N. A., E. A. Grin, G. Chong, E. Minkley, A. N. Hock, Y. Yu, L. Bebout, E. Fleming, D. P. H€ader, C. Demergasso, J. Gibson, L. Escudero, C. Dorador, D. Lim, C. Woosley, R. L. Morris, C. Tambley, V. Gaete, M. E. Galvez, E. Smith, I. Uskin-Peate, C. Salazar, G. Dawidowicz and J. Majerowicz (2009) The high-lakes project. *J. Geophys*. Res. 114, G00D08.

9. Cabrol, N. A., U. Feister, D. P. Hader, H. Piazena, E. A. Grin and A. Klein (2014) Record solar UV irradiance in the tropical Andes. *Front Environ Sci*. 2:19.

10. Agogué, H., F. Joux, I. Obernosterer and P. Lebaron (2005) Resistance of marine bacterioneuston to solar radiation. *Appl. Environ. Microbiol*. 71,5282–5289

11. Hernández, K. L., R. A. Quiñones, G. Daneri, M. E. Farias and E. W. Helbling (2007). Solar UV radiation modulates daily production and DNA damage of marine bacterioplankton from a productive upwelling zone (36◦S), Chile. *J.Exp.Mar.Bio.Ecol*.343,82–95

12. Mitchell, D. L. and D. Karentz. (1993). The induction and repair of DNA photodamage in the environment, p. In A. R. Young, L. O. Bjorn J. Moan, and W. Nultsch (ed.),.*Environmental UV photobiology. Plenum Press.* 345–377

13. Friedberg, E.C., G.C. Walker and W. Siede (1995). DNA Repair and Mutagenesis. Second edition. *ASM Press*,2005

14. Demergasso, C., C. Dorador, D. Meneses, J. Blamey, N. Cabrol, L. Escudero and G. Chong(2010) Prokaryotic diversity pattern in high-altitude ecosystems of the Chilean Altiplano. *J Geophys Res Biogeosciences.* 115:G00D09.

15. Dorador.C., D. Meneses, V. Urtuvia, C.Demergasso, I. Vila, K-P. Witzel and J. F. Imhoff (2009) Diversity of Bacteroidetes in high-altitude saline evaporitic basins in northern Chile. *J Geophys Res Biogeosciences*.;Res., 114, G00D05,

16. Fernández-Zenoff, M. V., M. C. Estévez and M. E. Farías (2014). Diurnal variation in bacterioplankton composition and DNA damage in the microbial community from an Andean oligotrophic lake. *Rev Argent Microbiol*. 46(4):358-362..

17. Flores, M. R., O. F. Ordonez, M. J. Maldonado and M. E. Farias (2009) Isolation of UV-B resistant bacteria from two high altitude Andean lakes (4,400 m) with saline and non saline conditions, *J. Gen. Appl. Microbiol*. 55, 447– 458.

18. Bequer Urbano, S., V. H. Albarracín, O. F. Ordoñez, M. E. Faríasand H. M. Alvarez (2013). Lipid storage in high-altitude Andean Lakes extremophiles and its mobilization under stress conditions in *Rhodococcus* sp. A5, a UV-resistant actinobacterium. *Extremophiles.* 17(2):217-227.

19. Albarracín V. H., G. P. Pathak, T. Douki, J. Cadet, C. D. Borsarelli, W. Gärtner and M. E. Farías (2012). Extremophilic Acinetobacter Strains from High-Altitude Lakes in Argentinean Puna: Remarkable UV-B Resistance and Efficient DNA Damage Repair. *Orig Life Evol Biosph*. 42(2-3):201-221.

20. Gorriti M. F., G. M. Dias, L. A. Chimetto, A. R. Trindade-Silva, B. S. Silva, M. A. Mesquita, G. B. Gregoracci, M. E. Farias and C. Thompson (2014) Genomic and phenotypic attributes of novel salinivibrios from stromatolites, sediment and water from a high altitude lake. *BMC Genomics*. 15(1):473.

21. Rasuk M. C., G. M. Ferrer, D. Kurth, L. R. Portero, M. E. Farías and V. H. Albarracín (2017) UV-Resistant Actinobacteria from High-Altitude Andean Lakes: Isolation, Characterization and Antagonistic Activities. *Photochem Photobiol*. 93(3):865-880.

22. Albarracín V., W. Gärtner and M. E. Farias (2013). UV Resistance and Photoreactivation of Extremophiles from High-Altitude Andean Lakes. *J Photochem Photobiol B*. 4-2013; 1-4.

23. Quaite, F. E., S. Takayanagi, J. Ruffini, J. C. Sutherland and B. M. Sutherland (1994). DNA damage levels determine cyclobutyl pyrimidine dimer repair mechanisms in alfalfa seedlings. *The Plant Cell*, 6(11), 1635-1641.

24. Simonson, C. S., T. A. Kokjohn and R. V. Miller (1990). Inducible UV repair potential of Pseudomonas aeruginosa PAO. *Microbiology*, 136(7), 1241-1249.

25. Weber S. (2005) Light-driven enzymatic catalysis of DNA repair: a review of recent biophysical studies on photolyase. *Biochim Biophys Acta* 1707: 1-23.

26. Kavakli, I. H., I. Baris, M. Tardu, S. Gül, H. Öner, S. Çal, S. Bulut, D. Yarparvar, Ç. Berkel, P. Ustaoğlu and C. Aydın (2017), The Photolyase/Cryptochrome Family of Proteins as DNA Repair Enzymes and Transcriptional Repressors. *Photochem Photobiol*, 93: 93–103.

27. Liu Z., L. Wang, and D. Zhong (2015). Dynamics and mechanisms of DNA repair by photolyase. *Physical chemistry chemical physics* : PCCP. 17(18):11933-11949.

28. Sancar A (2003) Structure and function of DNA photolyase and cryptochrome blue-light photoreceptors. *Chem Rev* 103:2203–2237

29. Chaves, I., R. M. Nijman, M. A. Biernat, M. I. Bajek, K.Brand, A. C. da Silva and G. T. van der Horst (2011). The Potorous CPD photolyase rescues a cryptochrome-deficient mammalian circadian clock. *PLoS One*, 6(8), e23447.

30. Roenneberg, T., and M. Merrow (2005). Circadian clocks—the fall and rise of physiology. *Nature Reviews Molecular Cell Biology*, 6(12), 965-971.

31. Harmer, S. L. (2009). The circadian system in higher plants. Annual review of plant biology, 60, 357-377.

32. Oberpichler, I., A. J. Pierik, J. Wesslowski, R. Pokorny, R. Rosen, M. Vugman, F. Zhang, O. Neubauer, E. Z. Ron and A. Batschauer (2011) A photolyase-like protein from Agrobacterium tumefaciens with an iron-sulfur cluster. PLoS One 6, e26775.

33. Kumar S., G. Stecher and K. Tamura (2015) MEGA7: Molecular Evolutionary Genetics Analysis version 7.0. *Molecular Biology and Evolution* (submitted).

34. Pokorny, R., T. Klar, U. Hennecke, T. Carell, A. Batschauer and L. O. Essen (2008). Recognition and repair of UV lesions in loop structures of duplex DNA by DASH-type cryptochrome. *Natl Acad Sci.* 105(52), 21023-21027.

35. Ordoñez, O. F., E. Lanzarotti, D. Kurth, M. F. Gorriti, S. Revale, N. Cortez, M. P. Vazquez, M. E. Farias and A. G. Turjanski (2013) Draft genome sequence of the polyextremophilic Exiguobacterium sp. Strain S17, isolated from Hyperarsenic Lakes in the Argentinian Puna. *Genome Announc*. 1, e01059–13.

36. Kurth D., C. Belfiore, M. F. Gorriti, N. Cortez, M. E. Farias and V. H. Albarracín (2015) Genomic and proteomic evidences unravel the UV-resistome of the poly-extremophile Acinetobacter sp. Ver3. *Front. Microbiol*. 6:328.

37. Albarracin VH, W. Gartner and M. E. Farias (2013). UV resistance and photoreactivation of extremophiles from high-altitude Andean lakes. In: Smith KC (ed) *The Science of Photobiology.* American Society for Photobiology

38. Farias M. E., N. Rascovan, D. M. Toneatti, V. H. Albarracin, M. R. Flores, D. G. Poire, M. M. Collavino, O. M. Aguilar, M. P. Vazquez and L. Polerecky (2013) The discovery of stromatolites developing at 3,570 m above sea level in a High-Altitude volcanic Lake Socompa, Argentinean Andes. *PLoS One*, 8, e53497.

39. Di Capua, C., A. Bortolotti, M. E. Farias and N. Cortez (2011) UV-resistant Acinetobacter sp. isolates from Andean wetlands display high catalase activity. *FEMS Microbiol*. Lett. 317, 181–189

40. Aziz, R. K., D. Bartels, A. A. Best, M. DeJongh, T. Disz and R. A. Edwards (2008). The RAST server: rapid annotations using subsystems technology. *BMC Genomics* 9:75.

41. Overbeek, R., R. Olson, G. D. Pusch, G. J. Olsen, J. J. Davis and T. Disz (2014). The SEED and the rapid annotation of microbial genomes using subsystems technology (RAST). *Nucleic Acids Res*. 42, D206–D214

42. Benson D.,A., I. Karsch-Mizrachi, D. J. Lipman, J. Ostell and D. LWheeler (2005) GenBank. *Nucleic Acids* Res. 33(Database issue):D34-8.

43. Lefort, V., Desper, R., Gascuel, O., (2015) FastME 2.0: A Comprehensive, Accurate, and Fast Distance-Based Phylogeny Inference Program. *Molecular Biology and Evolution*. 32(10), 2798–2800

44. Berman H. M., T. N. Bhat, P. E. Bourne, Z. Feng, G. Gilliland, G. Weissig and J. Westbrook (2000) The Protein Data Bank and the challenge of structural genomics. *Nat Struct Biol*. 7(11s):957-959.

45. Shen M. and A. Sali (2006) Statistical potential for assessment and prediction of protein structures. *Protein Sci*.2507-2524.

46. Chen V. B., W. B. Arendall III, J. J. Headd, D.A. Keedy, R. M. Immormino, G. J.Kapral, L. W. Murray, J. S. Richardson and D. C. Richardson (2012) MolProbity : all-atom structure validation for macromolecular crystallography. *International Tables for Crystallography*. Vol. F, ch. 21.6, pp. 694-701

47. Wiederstein M. and M. J.Sippl (2007). ProSA-web: interactive web service for the recognition of recognition of errors in three-dimensional structures of proteins.35(Web Server):W407-W410.

48. Shi W, T. Takano and Liu S (2012). Isolation and characterization of novel bacterial taxa from extreme alkali-saline soil. World J Microbiol Biotechnol. 2012;28(5):2147-2157

49. Li, W. J., H. H. Chen, Y. Q. Zhang, P. Schumann, E. Stackebrandt, L. H. Xu and C. L. Jiang (2004). Nesterenkonia halotolerans sp. nov. and Nesterenkonia xinjiangensis sp. nov., actinobacteria from saline soils in the west of China. *Int.J. Syst. Evol. Microbiol*. 54(3), 837-841.

50. Yamamoto K., M. Satake andH. Shinagawa (1984) A multiply phr-plasmid increases the ultraviolet resistance of a recA strain of Escherichia coli. Mutat Res Repair Reports. 131(1):11-18.

51. Sancar A., K. A. Franklin and G. B. Sancar (1984) Escherichia coli DNA photolyase stimulates uvrABC excision nuclease in vitro. Proc Natl Acad Sci U S A. 81(23):7397-7401.

52. Sancar G.B. andF. W. Smith (1989). Interactions between yeast photolyase and nucleotide excision repair proteins in Saccharomyces cerevisiae and Escherichia coli. *Mol Cell Biol*. 9(11):4767-4776.

53. Zenoff V. F., J. Heredia, M. Ferrero, F. Siñeriz and Farías M. E. (2006) Diverse UV-B Resistance of Culturable Bacterial Community from High-Altitude Wetland Water. *Curr Microbiol*. 2006;52(5):359-362.

54. Kirti K., S. Amita, S. Priti, A. Mukesh Kumar and S. Jyoti (2014) Colorful World of Microbes: Carotenoids and Their Applications. Adv Biol. 2014:1-13.

55. Dieser M., M. Greenwood, C. M. Foreman (2010) Carotenoid Pigmentation in Antarctic Heterotrophic Bacteria as a Strategy to Withstand Environmental Stresses. Arctic, Antarct Alp Res. 42(4):396-405.

56. Gao Q, F. Garcia-Pichel (2011) Microbial ultraviolet sunscreens. Nat Rev Microbiol. 9(11):791-802.

57. Galasso C., C. Corinaldesi, C. Sansone and C. Sansone (2017). Carotenoids from Marine Organisms: Biological Functions and Industrial Applications. Antioxidants ;6(4):96.

58. Singh OV and P. Gabani (2011) Extremophiles: radiation resistance microbial reserves and therapeutic implications. *J Appl Microbiol.* 110(4):851-861.

59. Singh S.P., D.P. Häder and R. P. Sinha (2010). Cyanobacteria and ultraviolet radiation (UVR) stress: Mitigation strategies. *Ageing Res Rev*. 9(2):79-90.

60. de la Coba F., J. Aguilera, M. V. de Gálvez, M. Álvarez, E. Gallego, F. L. Figueroa and E. Herrera(2009). Prevention of the ultraviolet effects on clinical and histopathological changes, as well as the heat shock protein-70 expression in mouse skin by topical application of algal UV-absorbing compounds. *J Dermatol Sci*. 55(3):161-169.

61. Sinha R.P. and D. P Häder D. P (2008). UV-protectants in cyanobacteria. Plant Sci. 174(3):278-289.

62. Proteau P. J., W. H. Gerwick, F. Garcia-Pichel and R. Castenholz (1993). The structure of scytonemin, an ultraviolet sunscreen pigment from the sheaths of cyanobacteria. Experientia. 49(9):825-829.

63. Soule T., F. Garcia-Pichel and V. Stout (2009). Gene expression patterns associated with the biosynthesis of the sunscreen scytonemin in Nostoc punctiforme ATCC 29133 in response to UVA radiation. *J Bacteriol*. 191(14):4639-4646.

64. Ekebergh A., P. Sandin and J. Martensson (2015). On the photostability of scytonemin, analogues thereof and their monomeric counterparts. *Photochem Photobiol Sci*. 14(12):2179-2186.

65. Lentzen G. and T. Schwarz (2006). Extremolytes: natural compounds from extremophiles for versatile applications. *Appl Microbiol Biotechnol*. 72(4):623-634.

66. Shahmohammadi H. R., E. Asgarani, H. Terato, T. Saito, Y. Ohyama, K. Gekko, O. Yamamoto and H. Ide (1998). Protective Roles of Bacterioruberin and Intracellular KCl in the Resistance of Halobacterium salinarium against DNA-damaging Agents. *J Radiat Res*. 39(4):251-262.

67. Saito T., Y. Miyabe and H. Ide (1997). Hydroxyl radical scavenging ability of bacterioruberin. *Radiat. Phys. Chem.*50, pp. 267-269.

68. Poppel, M. T., E. Skiebe, M. Laue, H. Bergmann, I. Ebersberger, T. Garn and G. Wilharm (2016). Acinetobacter equi sp. nov., isolated from horse faeces. *International journal of systematic and evolutionary microbiology*, 66(2), 881-888.

69. Geisselbrecht, Y., S. Fr€uhwirth, C. Schroeder, A. J. Pierik, G. Klug and L. O. Essen (2012) CryB from Rhodobacter sphaeroides: A unique class of cryptochromes with new cofactors. *EMBO Rep*. 13, 223–229.

70. Zhang F., P. Scheererb, I. Oberpichlera, T. Lampartera and Norbert Kraußc (2013) Crystal structure of a prokaryotic (6-4) photolyase with an Fe-S cluster and a 6, 7-dimethyl-8-ribityllumazine antenna chromophore. *Natl Acad Sci*. 2013. 110/18/7217

71. Zadow A., E. Ignatz, R. Pokorny, L. Essen and G. Klug (2016). Rhodobacter sphaeroides CryB is a bacterial cryptochrome with (6–4) photolyase activity. *The FEBS Journal* 283, 4291–4309.

72. Selby C., and A. Sancar (2006). A cryptochrome/photolyase class of enzymes with single-stranded DNA-specific photolyase activity. Natl Acad Sci. 103/47/17696.

73. Brudler R., K. Hitomi, H. Daiyasu, H. Toh, K. Kucho, M. Ishiura, M. Kanehisa, V. Roberts, K. Todo, J. Tainer and E. Getzoff (2003). Identification of a New Cryptochrome Class: Structure, Function, and Evolution. *Mol Cell*. 11(1):59-67.

74. Daiyasu H., T. Ishikawa, K. Kuma, S.Iwai, T. Todo andH. Toh (2004). Identification of cryptochrome DASH from vertebrates. *Genes to Cells*. 9(5):479-495.

75. Scheerer P., F. Zhang, J. Kalms, D. von Stetten, N. Krauss and I. Oberpichler (2015) The class III cyclobutane pyrimidine dimer photolyase structure reveals a new antenna chromophore binding site and alternative photoreduction pathways. *J BiolChem* 290, 11504–11514.

76. Schneider T. D. and Stephens R. M.(1995)Sequence logos: a new way to display consensus sequences. *Nucleic Acids Res*. 18(20). 18-20-6097.

77. Lin C, Todo T. (2005) The cryptochromes. Genome Biol. 2005;6(5).

78. Aubert C., P.,Mathis, A. P. Eker, K. Brettel, K. Hitomi and T. Todo (1999). Intraprotein electron transfer between tyrosine and tryptophan in DNA photolyase from Anacystis nidulans. Proc Natl Acad Sci U S A. 96(10):5423-5427.

79. Weber S., C. Kay, H. Mogling, K. Mobius, K. Hitomi and T. Todo (2002) Photoactivation of the flavin cofactor in Xenopus laevis (6-4) photolyase: Observation of a transient tyrosyl radical by time-resolved electron paramagnetic resonance. Proc Natl Acad Sci. 99(3):1319-1322.

80. Holub D., H. Ma, N. Krauß, T. Lamparter, M. Elstner, N. Gillet (2018) Functional role of an unusual tyrosine residue in the electron transfer chain of a prokaryotic (6–4) photolyase. Chem Sci. 9(5):1259-1272.

81. Brettel, k., and Byrdin, M. (2010). Reaction mechanisms of DNA photolyase. Current opinion in structural biology, 20(6), 693-701.

82. Müller M. and T. Carell (2009). Structural biology of DNA photolyases and cryptochromes. Curr Opin Struct Biol. 19(3):277-285.

83. Schleicher, E., B. Heßling, , V. Illarionova, A. Bacher, S. Weber, G. Richter and K. Gerwert (2005). Light- induced reactions of Escherichia coli DNA photolyase monitored by Fourier transform infrared spectroscopy. *The FEBS journal*, 272(8), 1855-1866.

84. Shepard E., and Broderick J. (2010) S-Adenosylmethionine and Iron–Sulfur Clusters in Biological Radical Reactions: *The Radical SAM Superfamily*. 2010.

85. Broach R. B., and Jarrett J. T. (2006). Role of the [2Fe-2S] 2+ cluster in biotin synthase: mutagenesis of the atypical metal ligand arginine 260. *Biochemistry*, 45(47), 14166-14174.

86. Zu, Y., Couture, M. M. J., Kolling, D. R., Crofts, A. R., Eltis, L. D., Fee, J. A., and Hirst, J. (2003). Reduction potentials of Rieske clusters: importance of the coupling between oxidation state and histidine protonation state. *Biochemistry*, 42(42), 12400-12408

87. Komori, H., R. Masui, S. Kuramitsu, S. Yokoyama, T. Shibata, Y. Inoue and K. Miki. (2001) Crystal structure of thermostable DNA photolyase: Pyrimidine-dimer recognition mechanism. *Proc. Natl. Acad. Sci.* U. S. A. 98, 13560–13565.

88. Albarracín V.H., J. Simon J, G. P. Pathak,L. Valle, T. Douki,J. Cadet, C. D. Borsarelli, M. E. Farias and Gärtner W (2014). First characterisation of a CPD-class I photolyase from a UV-resistant extremophile isolated from High-Altitude Andean Lakes. *Photochem. Photobiol. Sci.*,2014, 13, 739

89. Kiontke S., Y. Geisselbrecht, R. Pokorny, T. Carell, A. Batschauer and L. O. Essen (2011) Crystal structures of an archaeal class II DNA photolyase and its complex with UV-damaged duplex DNA. *EMBO J.* 30, 4437–4449

90. Miyazawa Y., H. Nishioka, K. Yura and T. Yamato (2008) Discrimination of Class I Cyclobutane Pyrimidine Dimer Photolyase from Blue Light Photoreceptors by Single Methionine Residue. *Biophysical Journal*. 94, 2194–2203.

91. Lucas-Lledo J. I., and M. Lynch (2009) Evolution of mutation rates: phylogenomic analysis of the photolyase/ cryptochrome family. *Molecular Biology and Evolution* 26, 1143–1153

92. Ueda T., A. Kato, S. Kuramitsu, H. Terasawa and I. Shimada (2005) Identification and characterization of a second chromophore of DNA photolyase from Thermusthermophilus HB27. *J BiolChem* 280, 36237–36243.

93. Oshima T. and K. Imahori (1971) Isolation of an Extreme Thermophile and Thermostability of its Transfer Ribonucleic and Acid and Ribosomes. *J. Gen. Appl. Microbiol.,* 17, 513-517.

94. Nobre M.F., H. G. Truper and M.S. Da Costa (1996) Transfer of Thermusruber (Loginova et al. 1984), Themussilvanus (Tenreiro et al. 1999), and Themuschliarophilus (Tenreiro et al. 1995) to Meiothemzus gen. nov. as Meiothermusruber comb. nov., Meiothermussilvanus comb. nov., and Meiothermuschliarophilus comb. nov., Respectively, and Emendation of the Genus Thermus. *Int J SystBacteriol* 46: 604–606

95. Eker A. P. M., R. H. Dekker and W.Berends (1981). Photoreactivating enzyme from Streptomyces griseus—IV. On the nature of the chromophore cofactor in Streptomyces griseusphotoreactivating enzyme. *Photochem Photobiol*. 33:65–72.

96. Kobayashi, T., M. Takao, A. Oikawa and A.Yasui (1989). Molecular characterization of a gene encoding a photolyase from Streptomyces griseus. *Nucleic Acids Res*. 17, 4731–4744.

97. Kanai S., R. Kikuno, H. Toh,H. Ryo and T. Todo (1997) Molecular evolution of the photolyase-blue-light photoreceptor family. *Journal of Molecular Evolution* 45, 535–548.

98. Chater K.F (2006) *Streptomyces* inside-out: a new perspective on the bacteria that provide us with antibiotics. *Philos Trans R SocLond B Biol Sci*.361:761–8.

99. BerdyJ. (2005). Bioactive microbial metabolites, a personal view. *J. Antibiot*. 58, 1–26

100. Hopwood D. A. (2006). Soil to genomics: the Streptomyces chromosome. *Annu. Rev. Genet.* 40, 1–23.

101. Matallana-Surget S., J. A. Meador, F. Joux and T. Douki (2008) Effect of the GC content of DNA on the distribution of UVB-induced bipyrimidine photoproducts. *Photochem. Photobiol. Sci.* 7, 794–801

102. Matallana-Surget S., T. Douki, R. Cavicchioli and F. Joux (2009) Remarkable resistance to UVB of the marine bacterium Photobacteriumangustum explained by an unexpected role of photolyase. *Photochem. Photobiol. Sci*. 8, 1313–1320.

103. O'Connor K.A., M. J. McBride, M. West, H. Yu, L. Trinh, K. Yuan, T. Lee and D. R. Zusman (1996). Photolyase of Myxococcusxanthus, a Gram-negative eubacterium, is more similar to photolyases found in Archaea and "higher" eukaryotes than to photolyases of other eubacteria. *J Biol Chem.* Mar 15; 271(11):6252–6259.

Tables

Table 1. HAAL's photoreceptors with sequence homology to Phr/Cry proteins found in genomes from Ver3, S17 and Act20.

HAAL´s Extremophiles	Name Protein	Putative Photoreceptor type according to phylogenetic analysis	RAST ID/Number of aa/Size	Identity with the closest protein in the database
Acinetobacter **sp. Ver3**	**Ver3Phr**	**CPD I Photolyase**	fig| 469.9.peg.1747 - pb: 1413; aa: 471 ; 54,98 kDa	deoxyribodipyrimidine photolyase _ *Acinetobacter* sp. VT 114 (WP_054581756) **67%**
	Ver3Cry	**FeS-BCP**	fig| 469.9.peg.2498 - pb: 1524; aa: 508 ; 59,58 kDa	deoxyribodipyrimidine photolyase _ *Acinetobacter* sp. VT 511 (WP_048881868) **95%**
Exiguobacterium **sp. S17**	**S17Phr**	**CPD I Photolyase**	fig|856854.4.peg.1656 - pb: 1356; aa: 452 ; 52,69 kDa	deoxyribodipyrimidine photolyase - *Exiguobacterium mexicanum* - (WP_034777040) **83%**
	S17Cry	**FeS-BCP**	fig|856854.4.peg.109 - pb: 1482; aa: 494 ; 57,44 kDa	deoxyribodipyrimidine photo-lyase - *Exiguobacterium pavilionensis* - (WP_021066163) **84%**
	S17CryD	**Cry-DASH**	fig|856854.4.peg.970 - pb: 1215; aa: 405 ; 47,19 kDa	photolyase - *Exiguobacterium alkaliphilum* - (WP_034817977) **79%**
Nesterenkonia **sp. Act20**	**Act20Phr**	**CPD III Photolyase**	fig|57494.15.peg.386 - pb: 1389; aa: 463 ; 52,67 kDa	deoxyribodipyrimidine photolyase - *Nesterenkonia* sp. AN1 - (WP_036475602) **83%**
				deoxyribodipyrimidine photolyase - *Arthrobacter* sp. A3 - (WP_044579450) **57%**
	Act20Cry	**FeS-BCP**	fig|57494.15.peg.1960 - pb: 1635; aa: 545 ; 61,6 kDa	deoxyribodipyrimidine photolyase - *Nesterenkonia* sp. AN1 - (WP_036477144) **75%**
				deoxyribodipyrimidine photolyase - *Arthrobacter* sp. Br18 - (WP_026550611) **69%**

Table 2. Z-score of the generated models and the corresponding templates.

Strain	Photorreceptor	Z-score		
		Models	Template	
Ver3	Phr CPD-I	-10,02	-11,47	1DNP
	Cry FeS-BCP	-10,17	-10,88	4DJA
S17	Phr CPD-I	-8,92	-11,47	1DNP
	Cry FeS-BCP	-10,82	-10,88	4DJA
	Cry CryDASH	-7,82	-10,73	1NP7
Act20	Phr CPD-III	-8,97	-11,59	4U63
	Cry FeS-BCP	-8,97	-10,42	3ZXS

Figure and Table Legends

Figure 1. **A.** Geographic position of the High Altitude Andean Lakes in the Central Andes, South America. **B-D.** Map localization and landscapes of L. Socompa and L. Verde. Macroscopic and microscopic view of HAAL's strains: E. *Acinetobacter* sp. Ver3; **F**. *Exiguobacterium* sp. S17; **G**. *Nesterenkonia* sp. Act20.

Figure 2. Absorption spectra of pigments, *Acinetobacter* sp. Ver3 (blue); *Exiguobacterium* sp. S17 (red); *Nesterenkonia* sp. Act20 (green).

Figure 3. UV resistance profile during increase UV-doses (up to 120 min): **A.** *Acinetobacter spp.* strains *(*Ver3, DSM 6963, DSM 30007, DSM 2463); **B.** *Exiguobacterium* spp. strains (S17, DSM 6208); **C.** *Nesterenkonia* spp. strains (Act20, DSM 15474). Photo-reactivation assays after UV-exposition of bacterial cultures: **D.** Ver3, DSM 6963, DSM 30007, DSM 2463 (UV-B dose: 6.4 kJ m^{-2}); **E.** S17, DSM 6208; (UV-B dose: 9.7 kJ m^{-2}). **F.** Act20, DSM 15474. (UV-B dose: 12.9 kJ m^{-2}). Dt: Non-exposed control; UV: UV treatment; DR: dark-repair; PR: photo repair. Each experiment consisted of three biological replicas, error bars are the standard deviation (Ó 2).

Figure 4. A. Sequence alignment between photolyases and cryptochromes from *Acinetobacter* sp. Ver3, *Exiguobacterium* sp. S17, *Nesterenkonia* sp Act20 and *E. coli* CPD photolyase Class I. Residues in direct interaction with the FAD chromophore and Tryptophan residues from the typical triad are indicated in green or red squares. **B.** Level of amino acid conservation for same alignment, using a Logo image with the distribution Kullback-Leibler, where the triad of tryptophan showed its conserved nature.

Figure 5. A. Sequence alignment of putative FeS-BCP cryptochromes from *Acinetobacter* sp. Ver3, *Exiguobacterium* sp. S17, *Nesterenkonia*sp Act20 and FeS-BCP of *R. sphaeroides*. Residues of cysteine that binds the 4Fe4S cluster are indicated by red squares. **B.** Level of amino acid conservation of cryptochromes, using a Logo image with the distribution Kullback-Leibler, cysteine bound to the FeS cluster are conserved.

Figure 6. A. Unrooted phylogenetic tree of Cryptochrome/Photolyase family members of the Bacteria domain generated using neighbor joining methods. Eight classes are identified, including two new groups: BCP-FeS (brown), Class II CPD photolyase (gray), Cry-DASH (purple), 8-HDF type class I CPD photolyase (red), MTHF type class I CPD photolyase (blue), Thermostable CPD photolyase (orange), Actinobacterial CPD photolyase (green) and Class III CPD photolyase (black). Photolyases were classified into 6 groups: photolyases with crystal structures (a), functionally expressed and characterized product (b), sequence characterized (c), function confirmed (d), function inferred by photoreactivation assays (e) and inferred by homology (f). The seven putative photolyase and cryptochrome sequences from *Acinetobacter* sp. Ver3, *Exiguobacterium* sp. S17 and *Nesterenkonia* sp Act20 are in bold and large print. Schemes of evolutionary process for the photolyase-cryptochrome family with **B.** Maximum Likelihood and **C.** Maximum Parsimony methods. Bootstrap values are shown in the trees and each step is explained in the text.

Figure 7. Models of the CPF members under study. **A.** Ver3Phr, **B.** Ver3Cry, **C.** S17Phr, **D.** S17CryD, **E.** S17Cry, **F.** Act20Phr, **G.** Act20Cry.

Figure 8. **A**. Superposition of the photolyase CPDs models; **B.** tryptophan triad; **C**. superposition of tryptophan triad of photolyase models. **D.** Superposition of the photolyase BCP-FeS models; **E.** amino acids that according (Cys) to the alignment bind the [FeS] clusters; **F**. superposition of cysteines from the BCP-FeS.

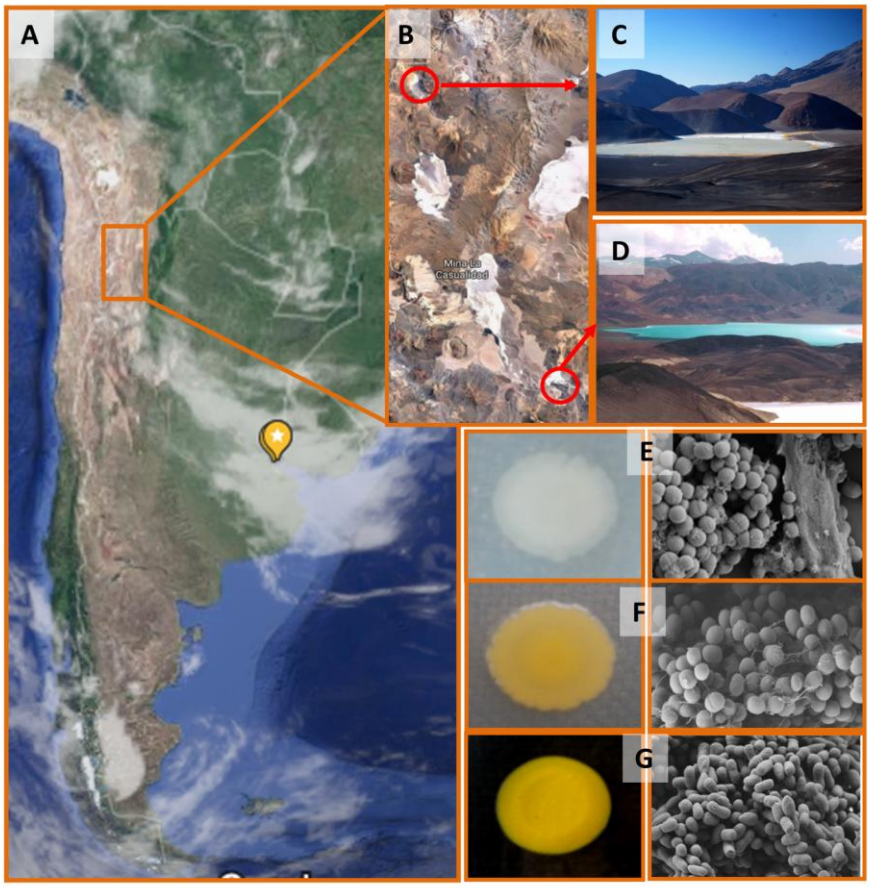

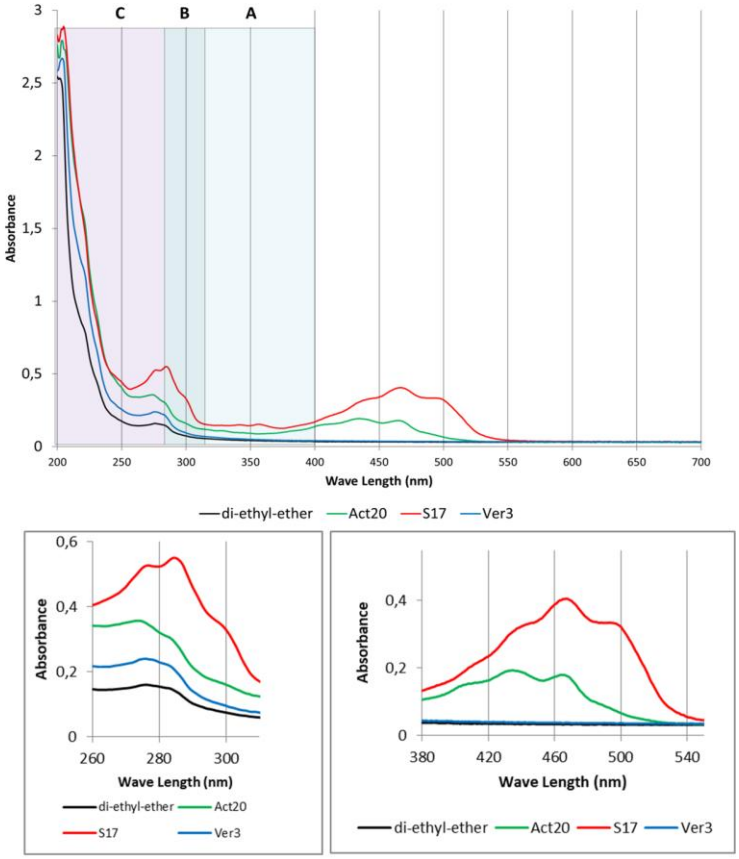

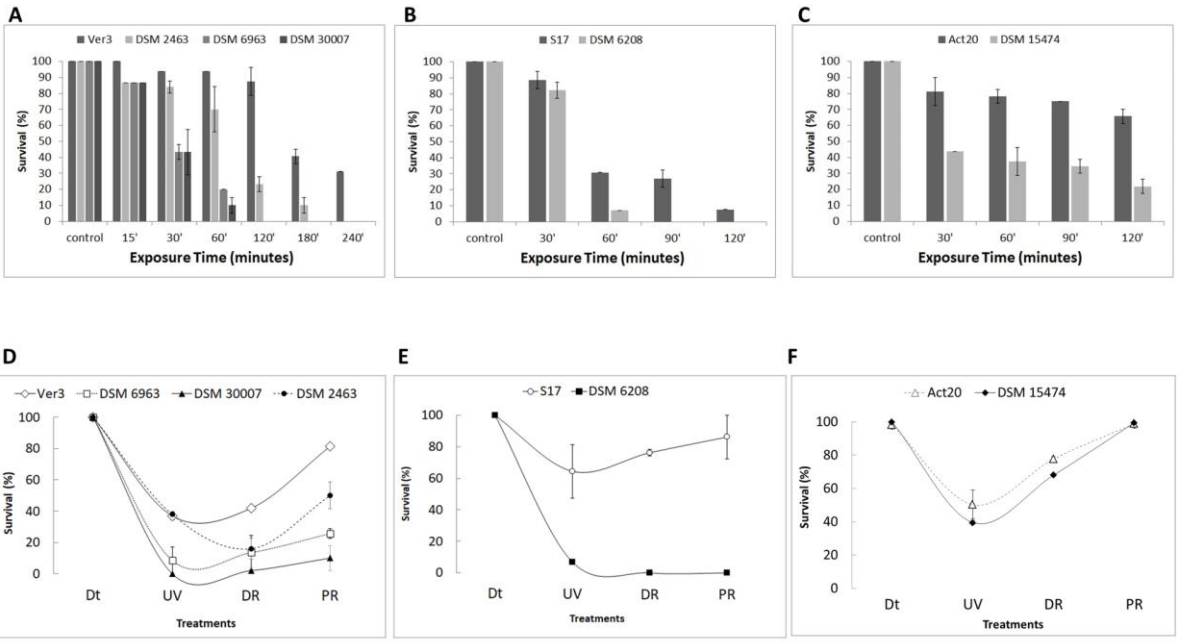

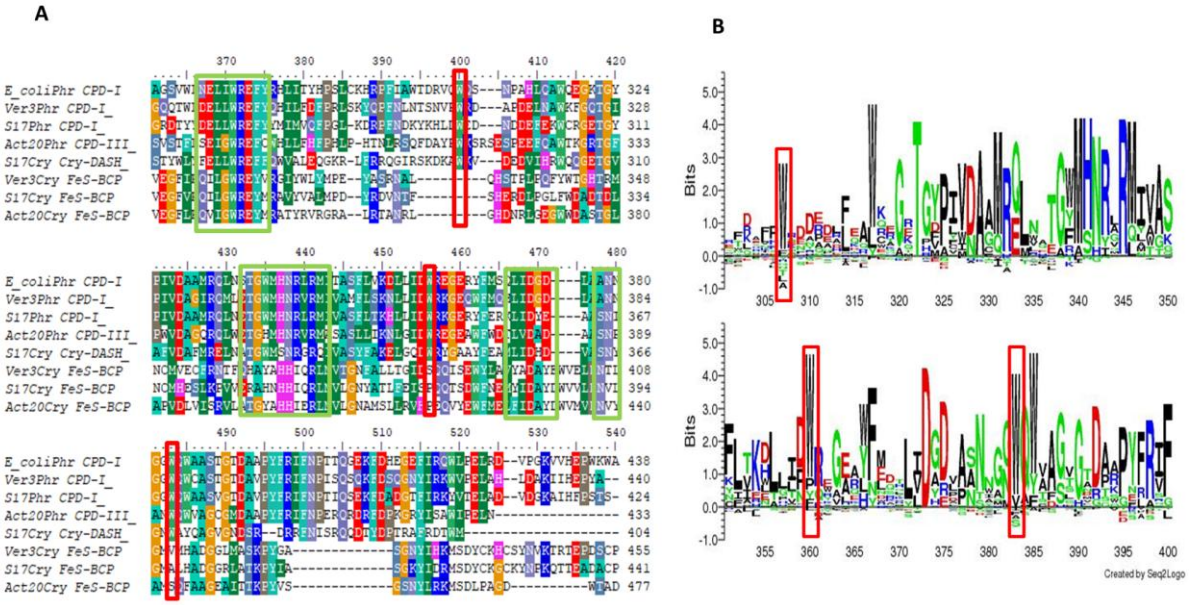

A

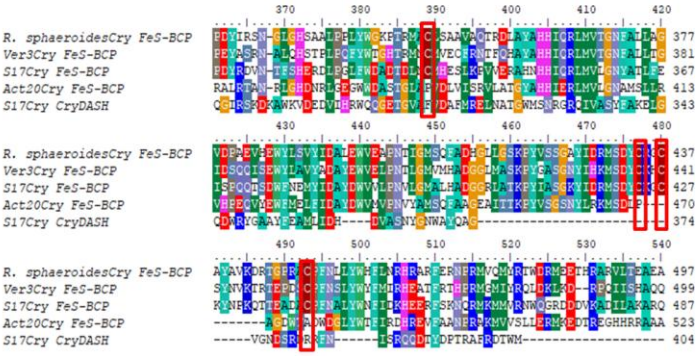

B